One-dimensional Bose gas on an atom chip

van Amerongen, A.H.

2 Theoretical background

2.1 Introduction

This chapter provides some theoretical background to the subsequent experimental chapters. The experimentally important concepts of magnetic trapping and evaporative cooling are briefly described. The main part of this chapter provides a summary of theory for the one-dimensional (1D) Bose gas at low temperature (and the cross-over to it from a 3D trapped gas) that is relevant for our experiment.

The 1D Bose system has attracted much interest because it has properties significantly different from that in higher dimensions. Counterintuitively, repulsive bosons in 1D become more *strongly* interacting with *decreasing* density. The theoretical description of such a many-particle system with strong interactions is challenging: As interactions increase in importance theoretical approaches that treat the gas as non interacting (ideal Bose gas) or weakly interacting (mean-field) break down. Already in the 1960s theorists were able to do much better, however. Helped by the simple symmetry of the 1D geometry Girardeau, Lieb and Liniger, and Yang and Yang were able to construct exact solutions for the many-body quantum system. Solutions were found for impenetrable bosons, known as the Tonks-Girardeau (TG) gas, by Girardeau [53] and for bosons with finite delta-function interaction by Lieb and Liniger [35] [54], using a Bethe Ansatz [55]. The model of 1D delta interacting bosons is integrable and therefore exactly solvable. Yang and Yang found analytic integral equations for the thermodynamics of the Lieb-Liniger gas [36] at any finite temperature and interaction strength. Their method is also known as the thermodynamic Bethe Ansatz.

With the spectacular advances in experiments with ultracold atomic gases in the 1990s this theoretical work became of experimental relevance and the first 1D condensates were realized in 2001 [39–41]. The importance of exactly solvable models for experiments with quantum gases was first pointed out by Olshanii in 1998 [33]. Until recently, however, most experimental attention was to the zero-temperature case of the Lieb-Liniger gas. In particular, there was a run to reach the strongly interacting Tonks-Girardeau (TG) gas. The TG regime was reached experimentally in 2004 in two groups. The group of Immanuel Bloch used a 2D optical lattice and added a weak periodic potential along the third axis to increase the effective mass of the bosons [42]. David Weiss and coworkers used a different laser scheme that removed the need for the complicating third periodic potential [43, 56–58]. It

was the paper by Kheruntsyan and coworkers [59] of 2003 that elaborated on the connection between Yang-Yang thermodynamics and cold atom experiments, the authors could identify new physical regimes using their exact calculations of the local pair correlation function.

Besides the strictly one-dimensional case, in practice many experiments [39, 50, 60] are performed in the cross-over from a three-dimensional to a one-dimensional system. Moreover, one works in a trap as opposed to the homogeneous case. The dimensional cross-over is of crucial importance in the description of our experimental data and is therefore given special attention in this chapter. In experiments on our trapped cold atomic clouds we turn two knobs: atom number and temperature. By turning these knobs we probe a variety of different physical regimes that are mostly separated by smooth cross-overs rather than sharp phase transitions. Besides the only true phase transition that we encounter: Bose-Einstein condensation, three cross-overs are met:

- cross-over from a three-dimensional to a one-dimensional system,
- cross-over from a decoherent to a coherent atomic sample in 1D,
- cross-over from a weakly interacting to a strongly interacting gas in 1D.

The outline of this chapter is as follows. Section 2.2 introduces the basics of magnetic trapping. In Sec. 2.3 the commonly used approach to the ideal Bose gas and the phenomenon of Bose-Einstein condensation is summarized. We discuss the homogeneous and trapped cases in 3D and 1D as well as the dimensional cross-over. Section 2.4 deals with weakly interacting (quasi-)condensates in 3D, in 1D and in the dimensional cross-over. Phase-fluctuating condensates, and the relation between the phase coherence length and the temperature of a quasi-condensate are studied in Sec. 2.4.4. Section 2.5 is dedicated to the exact results for 1D repulsive bosons by Tonks-Girardeau, Lieb-Liniger and Yang-Yang. In section 2.5.3 we present a new finite-temperature model that explains our experimentally obtained data very well (see also Ch. 6). The weakly interacting 1D gas is treated using the exact Yang-Yang thermodynamic solutions thus incorporating both the cross-over from a decoherent to a coherent system and the cross-over from weak to strong interactions. In Sec. 2.6 we give an overview of the discussed regimes that can be characterized by the three parameters: interaction strength, radial confinement and temperature. These parameters span a three dimensional space. We specifically describe two subspaces: (a) interaction strength versus radial confinement at $T = 0$ (Sec. 2.6.1); (b) interaction strength versus temperature in the 1D limit (Sec. 2.6.2). Section 2.7 briefly touches on previous models for finite-temperature degenerate systems. Finally, in Sec. 2.8 we give some theoretical background for the experimentally important tool of evaporative cooling.

2.2 Magnetic trapping

Magnetic trapping is due to the Zeeman effect: The energy of the atomic state depends on the magnetic field due to the interaction of the magnetic moment of the

atom with the magnetic field, for a detailed description see e.g. [61–63]. A Zeeman sublevel of an atom with given total electronic angular momentum J and nuclear spin I can be labelled by the projection m_F of the total atomic spin $\mathbf{F} \equiv \mathbf{I} + \mathbf{J}$ on the axis of the field $\mathbf{B}$ and by the total F ranging from $|I - J|$ to $I + J$. We are specifically dealing with the electronic ground state ($J = S = 1/2$) of ^{87}Rb ($I = 3/2$) so that $F = 1$ or $F = 2$. For these states the Zeeman energy shift can be calculated with the Breit-Rabi formula [63]. For the special case of atoms in the doubly polarized state ($F = 2, m_F = 2$) the Breit-Rabi formula yields a linear Zeeman shift

$$U(B) = U(0) + 2g_F\mu_B|\mathbf{B}|, \tag{2.1}$$

where $g_F \equiv (g_J + 3g_I)/4$, with $g_J = 2.00233113(20)$ [61] the fine structure Landé g-factor, $g_I = -0.0009951414(10)$ [61] the nuclear g-factor, $U(0)$ the energy in zero field and μ_B being the Bohr magneton. Because of the increasing energy in Eq. (2.1) with increasing magnetic field, atoms in the state ($F = 2, m_F = 2$) are "low-field seekers" that can be trapped in a local magnetic-field minimum. The other Zeeman states for ^{87}Rb that can be magnetically trapped for moderate field values are $F = 2, m_F = 1$ and $F = 1, m_F = -1$. In a region of small magnetic field the precession of the atomic magnetic moment is so slow that the changing field direction as a result of the atomic motion cannot be followed adiabatically. Atoms traversing such a region can undergo a so-called Majorana spin-flip to an untrapped state. To avoid this loss mechanism access of the atoms to low magnetic field regions should be prevented by arranging a non-zero magnetic field strength at the potential minimum.

To describe the thermodynamics of a trapped gas it is convenient for future reference to approximate the confining potential as a power-law trap of the general form [31]

$$U(x, y, z) = a_x|x|^{1/\delta_1} + a_y|y|^{1/\delta_2} + a_z|z|^{1/\delta_3}, \tag{2.2}$$

where

$$\delta = \sum_i \delta_i, \tag{2.3}$$

with $\delta = 0$ for 3D box-like, $\delta = 3/2$ for 3D harmonic and $\delta = 3$ for a spherical-quadrupole trap. The lowest order, and therefore tightest, magnetic trapping potential that has a non-zero minimum is 3D harmonic and can be written as

$$U(x, y, z) = U_0 + \frac{1}{2}m\omega_x^2x^2 + \frac{1}{2}m\omega_y^2y^2 + \frac{1}{2}m\omega_z^2z^2, \tag{2.4}$$

where ω_i is the single-particle oscillator frequency and m is the atomic mass.

A magnetic-field configuration that is 3D harmonic near the minimum was introduced by Ioffe [64] for plasma confinement. It was first proposed and used by Pritchard [65] to trap neutral atoms and is known as the Ioffe-Pritchard (IP) trap. Following Luiten [66] we define $\alpha = (\partial B_\perp/\partial\rho)_{x=x_0}$ and $\beta = (\partial^2 B_x(0, 0, x)/\partial x^2)_{x=x_0}$, and write the magnetic field for the IP configuration in polar coordinates

$$\begin{aligned} B_\perp(\rho, \phi, x) &= \alpha\rho\sin(2\phi) - \tfrac{1}{2}\beta\rho(x - x_0), \\ B_\phi(\rho, \phi, x) &= \alpha\rho\cos(2\phi), \\ B_\parallel(\rho, \phi, x) &= B_0 + \tfrac{1}{2}\beta(x - x_0)^2 - \tfrac{1}{4}\beta\rho^2. \end{aligned} \tag{2.5}$$

Indeed the magnetic field is approximately harmonic close to the center of the IP trap, for magnetic field values close to B_0 (the value of the magnetic field in the trap bottom). The harmonic approximation is valid for trapped atom clouds with a temperature much lower than $\mu_B B_0/k_B$. Using equations (2.1), (2.4) and (2.5) we find the trap frequencies in axial and radial direction

$$\omega_{\parallel} = \sqrt{\frac{\mu_B g_F m_F}{m}\beta}, \tag{2.6}$$

$$\omega_{\perp} = \sqrt{\frac{\mu_B g_F m_F}{m}(\frac{\alpha^2}{B_0} - \frac{\beta}{2})} \tag{2.7}$$

In the high-temperature limit, if the thermal energy of atoms in a IP-trap is much larger then the energy corresponding to the trap bottom, $k_B T \gg \mu_B B_0$, we can approximate the IP potential, resulting from Eq. (2.1) and Eq. (2.5), in the two radial directions by a linear and in the axial direction by a harmonic shape. The factor δ, Eq. (2.3), equals 5/2 in this case.

Strong trapping forces are generated by high magnetic field gradients. Weinstein and Librecht [47] realized that when creating a trapping field at a distance r from a wire that carries a current I, the field gradient scales as I/r^2. Microtraps thus provide an advantage over conventional electromagnets to tightly confine atoms.

The simplest wire-based trap is illustrated in Fig. 1.1. A current-carrying wire (along x) whose magnetic field is compensated by a homogeneous field B_{bias} (along y) forms a waveguide. Around the minimum (r_0), the field in the radial direction (yz-plane) is quadrupolar. This waveguide can be closed at the end points by adding two perpendicular current-carrying wires (along y) thus creating an **H**. End caps can also be made by bending the leads of the x-wire in the y-direction to create a **Z** shape. One can estimate the field gradient of such a trap using the field for an infinitely thin wire

$$r_0 = \frac{\mu_0}{2\pi}\frac{I}{B_{\text{bias}}}, \tag{2.8}$$

$$B'(r_0) = -\frac{\mu_0}{2\pi}\frac{I}{r_0^2}, \tag{2.9}$$

with $\mu_0 = 4\pi \cdot 10^{-7} N A^{-2}$. For example, with a current of 1 A and $B_{\text{bias}} = 100$ G we have $r_0 = 20$ μm and a huge gradient $B'(r_0) = 5 \cdot 10^4$ G/cm.

2.3 Ideal Bose gas

In the ideal-gas description, atoms are considered as non-interacting quantum-mechanical particles. For homogenous ultracold dilute Bose gases in 3D this description can be found in textbooks such as [67]. This treatment has been extended for power-law potentials [31, 68], and for lower dimensional systems [32, 69].

In a 3D homogenous gas of bosons the average occupation number N_i of states with energy ε_i obeys Bose statistics

$$N_i = \frac{1}{e^{\beta(\varepsilon_i - \mu)} - 1} = \frac{z e^{-\beta\varepsilon_i}}{1 - z e^{-\beta\varepsilon_i}}, \tag{2.10}$$

where $\beta = (k_B T)^{-1}$. The fugacity z and the chemical potential μ are related by $z = e^{\beta\mu}$. The total atom number N is found by summing over all quantum states i

$$N = \sum_{i=0}^{\infty} N_i. \tag{2.11}$$

This sum diverges for $z \to 1$ because the term $N_0 = z/(1-z)$ diverges in the thermodynamic limit (we take $\varepsilon_0 = 0$ from here on). Splitting off the diverging term N_0, replacing the rest of the sum by an integral (one state per phase space element $\Delta\mathbf{r}\Delta\mathbf{p} = h^3$) the equation of state for N atoms occupying a volume V becomes

$$\frac{N}{V} = \frac{4\pi}{h^3} \int_0^{\infty} dp\; p^2 \frac{1}{z^{-1} e^{\beta p^2/2m} - 1} + \frac{1}{V} \frac{z}{1-z}. \tag{2.12}$$

This can be written in the form [67]

$$n(z, T) = \frac{1}{\Lambda_T^3} g_{3/2}(z) + \frac{N_0}{V}, \tag{2.13}$$

where $n = N/V$ is the particle density,

$$\Lambda_T = \sqrt{2\pi\hbar^2/m k_B T}, \tag{2.14}$$

is the thermal de Broglie wavelength and $g_{3/2}$ is the Bose or Polylog function defined by

$$g_\alpha(z) = \sum_{j=1}^{\infty} z^j / j^\alpha. \tag{2.15}$$

For the ground-state particle density we have

$$\frac{N_0}{V} = n_0 = \frac{1}{V} \frac{z}{1-z} \tag{2.16}$$

and for the density in the excited states

$$n_e = \frac{1}{\Lambda_T^3} g_{3/2}(z). \tag{2.17}$$

Note that $g_{3/2}(z)$ is finite for $z \to 1$ ($g_{3/2}(1) = 2.612\ldots$), and thus n_e is limited, $n_e \leq g_{3/2}(1)/\Lambda_T^3$. At a given density, for low enough temperature, μ tends to zero from below and we have $z \to 1$; the Bose gas is saturated. All extra particles added at constant temperature will be accommodated in the ground state. The ground state becomes macroscopically occupied giving rise to the phenomenon of

Bose-Einstein condensation. At the transition, the critical density and temperature are

$$n_c = \frac{1}{\Lambda_T^3} g_{3/2}(1), \tag{2.18}$$

$$T_c = \frac{2\pi\hbar^2}{m k_B} \left(\frac{n}{g_{3/2}(1)} \right)^{2/3}. \tag{2.19}$$

A phase space density can be defined as the number of particles occupying a volume equal to the de Broglie wavelength cubed

$$\Phi = n\Lambda_T^3. \tag{2.20}$$

At the critical point the phase space density is $\Phi = g_{3/2}(1)$. We make use of Eq. (2.19) to write down the temperature dependence of the fraction of particles in the ground state

$$\frac{N_0}{N} = 1 - \left(\frac{T}{T_c} \right)^{3/2}. \tag{2.21}$$

Homogeneous 2D and 1D ideal gas

Unlike the 3D case, for a 2D system in the thermodynamic limit the population of the ground state remains microscopic for decreasing temperatures down to $T \to 0$. One can say that there is no BEC in a finite-temperature ideal homogeneous 2D Bose gas. Similarly in 1D, in the thermodynamic limit the population of the ground state remains microscopic for any T indicating the absence of BEC in this system.

One can define a degeneracy temperature T_d for lower-dimensional systems that indicates the transition from the classical regime to the regime where a quantum treatment is needed because the thermal de Broglie wavelength starts to exceed the average interparticle separation. For a homogeneous Bose gas in 1D the semiclassical approach yields

$$n(z, T) = \frac{1}{\Lambda_T} g_{1/2}(z), \tag{2.22}$$

the 1D equivalent of Eq. (2.13) for 3D. Note that $g_{1/2}(z)$ diverges as $z \to 1$, consistent with the absence of a macroscopically occupied ground state in 1D in the semiclassical approximation. Degeneracy for a one-dimensional homogeneous Bose gas is thus reached for

$$T_d = \frac{\hbar^2 n_1^2}{2 m k_B}, \tag{2.23}$$

where n_1 is the 1D density.

2.3.1 Ideal Bose gas harmonically trapped in 3D and 1D

We now turn to the D-dimensional ideal Bose gas in the presence of external harmonic confinement $V_{\text{ext}}(\mathbf{r}) = \sum_{i=1}^{D} m\omega_i^2 r_i^2/2$. We assume $k_B T \gg \hbar\omega_i$, consequently

we can use the semiclassical approximation and replace the sum in Eq. (2.11) by an integral. The semiclassical energy of the atoms trapped in the external potential is

$$\varepsilon(\mathbf{r},\mathbf{p}) = \frac{\mathbf{p}^2}{2m} + V_{\text{ext}}(\mathbf{r}). \tag{2.24}$$

The density distribution of the thermal atoms as a function of position and momentum respectively is then obtained by integration (over momentum and position respectively) yielding

$$n(\mathbf{r}) = \frac{1}{\Lambda_T^D} g_{D/2}\left[z e^{-\beta V_{\text{ext}}(\mathbf{r})}\right], \tag{2.25}$$

$$n(\mathbf{p}) = \frac{1}{(m\bar{\omega}\Lambda_T)^D} g_{D/2}\left[z e^{-\beta p^2/2m}\right], \tag{2.26}$$

where $\bar{\omega} = (\Pi_{i=1}^{D}\omega_i)^{1/D}$.

It was shown in [32] that upon lowering the dimension the critical temperature becomes higher. The expression for the critical temperature in a 1D trapped gas obtained in [32] is

$$N = \frac{k_B T_c}{\hbar\omega} \ln \frac{2k_B T_c}{\hbar\omega}. \tag{2.27}$$

2.3.2 Ideal Bose gas in the 3D-1D cross-over

If the 3D harmonic trap is highly anisotropic and needle shaped with $\omega_\perp \gg \omega_\parallel$ and $k_B T \approx \hbar\omega_\perp$ we have a cross-over from 3D to 1D for the ideal Bose gas. Only a few radial quantum states are occupied, therefore radially we can no longer use the semiclassical approximation from Sec. 2.3.1. In this cross-over case we sum explicitly over the radially exited states j of the harmonic oscillator with degeneracy $(j+1)$. For the axial direction we use the local density approximation (LDA): We treat the gas as locally homogeneous with a spatially varying chemical potential $\mu(x) = \mu - m\omega^2 x^2/2$ [70]. The resulting axial atomic density n_l is

$$n_l(x) = \sum_{j=0}^{\infty}(j+1)\frac{1}{\Lambda_T} g_{1/2}\left[e^{\beta(\mu(x)-j\hbar\omega_\perp)}\right]. \tag{2.28}$$

2.4 Weakly interacting (quasi-)condensate

Consider a harmonically trapped gas in the low temperature limit far below the condensation temperature: $T \ll T_c$ and $N_0/N \to 1$, i.e. we have an almost pure Bose-Einstein condensate. Nearly all particles occupy the ground state and the atomic density becomes high. When the interaction energy exceeds the harmonic oscillator level splitting we can no longer neglect the effect of interatomic interactions.

Bogoliubov [71] adopted a mean-field approach to approximate the many-body wavefunction for the weakly interacting Bose gas, in order to obtain the excitation

spectrum for the zero-temperature limit (see Sec. 2.4.4). For an inter-particle separation that is much larger than the range of the atomic interaction potential and for low collision energies atomic interactions can be described using only s-wave scattering. The mean-field interaction energy can then be written as $\mu = ng$, where n is the 3D atomic density and g the coupling constant

$$g = \frac{4\pi\hbar^2 a}{m}, \tag{2.29}$$

where a is the s-wave atomic scattering length ($a = 5.24$ nm for ^{87}Rb in the state $F = 2, m_F = 2$ [72]). The Gross-Pittaevski (GP) equation is a mean-field expression for the ground-state wavefunction ψ

$$\left[-\frac{\hbar^2}{2m}\nabla^2 + V_{\text{ext}}(\mathbf{r}) + g|\psi(\mathbf{r})|^2\right]\psi(\mathbf{r}) = \mu\psi(\mathbf{r}), \tag{2.30}$$

where $V_{\text{ext}}(\mathbf{r})$ is an external confining potential. Equation (2.30) is a non-linear Schrödinger equation, normalized as

$$N = \int d\mathbf{r}|\psi(\mathbf{r})|^2. \tag{2.31}$$

A Bose-Einstein condensate in the 3D mean-field regime is characterized by long-range order of the phase. The correlation length $l_c = \hbar/\sqrt{mng}$, the typical length scale associated with the atomic interaction energy, should be much smaller than the decay length of the phase coherence for any mean-field theory to hold.

2.4.1 Mean-field in three dimensions

We take the external potential in Eq. (2.30) to be a 3D isotropic harmonic trap $V_{\text{ext}}(\mathbf{r}) = m\omega^2\mathbf{r}^2/2$. A trapped Bose-Einstein condensate in the mean-field regime can be treated in the local density approximation (LDA) provided $\mu \gg \hbar\omega$. In this limit, the atomic density changes on a length scale much larger than that of the correlations in the gas, consequently we can treat the gas as locally homogeneous with a spatially varying chemical potential [70]. This amounts to neglecting the first (kinetic energy) term in Eq. (2.30); the mean-field energy of the trapped condensate exactly compensates the external potential energy. We have, for the spatial region where $V_{\text{ext}} < \mu_{TF}$, a cloud with a parabolic Thomas-Fermi (TF) profile in all three directions

$$n_{TF}(\mathbf{r}) = \frac{\mu_{TF} - V_{\text{ext}}(\mathbf{r})}{g}, \tag{2.32}$$

and $n_{TF} = 0$ elsewhere. The peak chemical potential μ_{TF} is determined by the total particle number N_0. For a harmonic potential, the result is

$$\mu_{TF} = \frac{\hbar\omega}{2}\left(\frac{15N_0 a}{l}\right)^{2/5}, \tag{2.33}$$

where $l = \sqrt{\hbar/m\omega}$ is the ground-state size.

2.4.2 Mean-field 1D

If in an ultracold gas under strong radial confinement the thermal energy drops below the radial level splitting ($k_B T \ll \hbar\omega_\perp$), the atomic motion in transverse directions is frozen and we speak of a one-dimensional system. For temperatures much lower than the degeneracy temperature ($T \ll T_d$) [Eq. (2.23)], and sufficiently high density we have a weakly interacting gas that can be treated similarly to the 3D case using a mean-field theory. The resulting 1D system exhibits quasi-long-range order of the phase at zero temperature (the phase coherence decays algebraically) [34]. Therefore we do not speak of a true condensate but rather of a quasi-condensate (under sufficient axial harmonic confinement full phase coherence can be regained, see Sec. 2.4.4). We can now write for the 1D mean-field interaction energy $\mu \approx g_1 n_1 \ll \hbar\omega_\perp$, where we use the effective 1D coupling found by Olshanii [33]

$$g_1 = \frac{2\hbar^2 a}{m l_\perp^2}\left(1 - \mathcal{C}\frac{a}{\sqrt{2}l_\perp}\right)^{-1}, \tag{2.34}$$

with the constant $\mathcal{C} = 1.4603\ldots$ [33] and the transverse oscillator length $l_\perp = \sqrt{\hbar/m\omega_\perp}$. In our experimental situation $l_\perp \gg a$ and the second term on the right-hand-side of Eq. (2.34) is a small correction. This 1D mean-field gas has the shape of the harmonic-oscillator ground state in the transverse direction. Along the axis we can use the LDA and find the parabolic Thomas-Fermi shape for the harmonically trapped case.

2.4.3 Mean-field 3D-1D crossover

The dimensional cross-over at $T = 0$ for a quasi-condensate with $\mu \approx \hbar\omega_\perp$ was treated in the mean-field regime by Menotti and Stringari [73] and by Gerbier [74]. The cross-over is approached from the 3D side where the chemical potential is much higher then the axial level splitting ($\mu \gg \hbar\omega_\parallel$): The condensate is in the GP regime and the density profile is parabolic both in axial and radial directions. Upon reduction of the linear density and consequently of the chemical potential we pass the dimensional cross-over regime ($\mu \approx \hbar\omega_\perp$) and reach the regime $\mu \ll \hbar\omega_\perp$. This results in a shape change of the radial density profile from parabolic when $\mu \gg \hbar\omega_\perp$ to the gaussian shape of the harmonic oscillator ground state for $\mu \ll \hbar\omega_\perp$. As long as $\mu \gg \hbar\omega_\parallel$ the *axial* shape stays parabolic. The characteristics of the condensate change gradually when going from elongated 3D to 1D. There is no transition point but a transition region. Gerbier [74] found a simple interpolation for the calculation of the chemical potential across the transition

$$\mu = \hbar\omega_\perp\left(\sqrt{1 + 4an_l} - 1\right), \tag{2.35}$$

where the local linear density n_l is used without information on the axial potential. This approximate function Eq. (2.35) yields values that were found to be very accurate in comparison with exact numerical results obtained by Menotti [75]. The linear density profile in the external axial potential $V_{\text{ext}} = m\omega_x^2 x^2/2$ can be found in

the local density approximation using[1]

$$n(x) = \frac{1}{4a}\frac{V_{\rm ext}(L)-V_{\rm ext}(x)}{\hbar\omega_\perp}\left[\frac{V_{\rm ext}(L)-V_{\rm ext}(x)}{\hbar\omega_\perp}+2\right], \tag{2.36}$$

$$L = \frac{l_x^2}{l_\perp}\sqrt{\frac{2\mu}{\hbar\omega_\perp}}, \tag{2.37}$$

where $l_{x,\perp}=\sqrt{\hbar/m\omega_{x,\perp}}$. We can define a cross-over point by equating the chemical potential Eq. (2.35) to the transverse oscillator strength ($\mu_{\rm co}=\hbar\omega_\perp$), yielding

$$n_{l,\rm co}=\frac{3}{4a}. \tag{2.38}$$

For ^{87}Rb in the $F=2, m_F=2$ state ($a=5.24$ nm) the cross-over to 1D is reached at a linear density $n_{l,\rm co}\approx 150\ \mu\text{m}^{-1}$.

2.4.4 Excitations in elongated quasi-condensates

This section follows the lines of the review article on low-dimensional trapped gases by Petrov and coworkers [76] and in particular their treatment of finite temperature excitations of condensates with fluctuating phase (quasi-condensates) in the 1D regime, that is relevant to the experiments described in this thesis. The treatment starts from the 1D case. Petrov *et al.* [77] showed that a similar treatment holds for elongated 3D condensates.

In the mean-field regime at $T=0$ long range order decays algebraically [28, 29]. At finite T, the phase coherence decays exponentially with a characteristic phase coherence length l_ϕ. In a trap, if l_ϕ exceeds the condensate halflength L, we have a true condensate. While for $l_\phi < L$ we have a quasi-condensate with fluctuating phase. In a quasi-condensate at sufficiently low temperatures so that $l_\phi \gg l_c$ density fluctuations are suppressed by the atomic interactions. The appearing phase fluctuations at finite temperature stem from thermal excitations of elementary modes of oscillation along the axis of the cloud. Bogoliubov [71] derived the excitation spectrum of a homogeneous weakly interacting Bose gas at zero temperature. His treatment was generalized for the spatially non-uniform case by de Gennes [78]. The Bogoliubov-de Gennes equations yield the energies of the elementary excitations of phase and density of the condensate

$$\varepsilon(k) = \sqrt{E(k)[E(k)+2\mu]}, \tag{2.39}$$

where $E(k)=\hbar^2k^2/2m$ is the free-particle spectrum. The spectrum Eq. (2.39) is phonon-like for energies in the order of or smaller than μ. The energies are $\varepsilon(k)\approx c_s\hbar k$, with the speed of sound $c_s=\sqrt{\mu/m}$. For larger momenta the spectrum is particle like with $\varepsilon(k)\approx E(k)+\mu$. At low enough temperature, $T\ll T_d,\mu$, the assumption that density fluctuations are small is justified. Then the fluctuations of

[1] In the 2004 article by Gerbier [74] there are a few typographical errors in the corresponding equations.

the phase alone follow the same phonon-like Bogoliubov-de Gennes equations [76]. The gas can be viewed as consisting of the sum of a macroscopic wave-function containing contributions with wave-vectors $k \ll 1/l_c$, with $l_c = \hbar/\sqrt{m\mu}$, and a small component including the contributions with $k \sim 1/l_c$.

Theory for excitations of quasi-condensates can be extended to include non-zero temperature in the Bogoliubov-Popov approach [79, 80]. Petrov *et al.* worked out the case of a harmonically trapped, phase-fluctuating condensate for 1D [34] and elongated 3D [77] systems. We repeat some of their results below.

Phase fluctuations originate from thermal excitations of Bogoliubov modes of oscillation along the condensate axis. The phase coherence length is inversely proportional to the quasi-condensate temperature, therefore l_ϕ can be used as a thermometer for phase fluctuating condensates

$$l_\phi = \frac{\hbar^2 n_1}{m k_B T}. \tag{2.40}$$

Below a temperature T_ϕ the phase coherence extends over the whole harmonically trapped cloud ($l_\phi = L$) and a true condensate is regained

$$T_\phi = \frac{\hbar^2 n_1}{m k_B L}. \tag{2.41}$$

The mean-field approach is not valid anymore at high temperatures or low densities such that $l_c \gtrsim l_\phi$. In that case the density fluctuates strongly like in a non-degenerate gas. It is important to point out here that these strong density fluctuations imply that the usual (perturbative) Bogoliubov approach to the degenerate gas must break down, since the Popov approximation (expanding the fluctuations around the average density) can no longer be relied upon. In the next section we will show that, luckily, for this regime exact solutions for the many-body wavefunction are known.

2.5 Exact solutions in 1D

This section discusses exactly solvable models for interacting bosons in 1D. Solutions were found for impenetrable bosons by Girardeau [53] and for bosons with finite delta-function interaction by Lieb and Liniger [35]. Remarkably, Yang and Yang found integral equations describing the thermodynamics of the Lieb-Liniger gas [36] at any finite temperature. Figure 2.1 shows a cartoon of atomic density distributions in 1D for $T = 0$ (adapted from Ref. [43]). For increasing values of the interaction parameter γ, the interatomic separation increases, and the size of the wave-functions decreases.

2.5.1 Tonks-Girardeau

For a system of impenetrable point-like bosons in 1D the wave-function and ground state energy were derived by Girardeau [53]. By definition impenetrability means

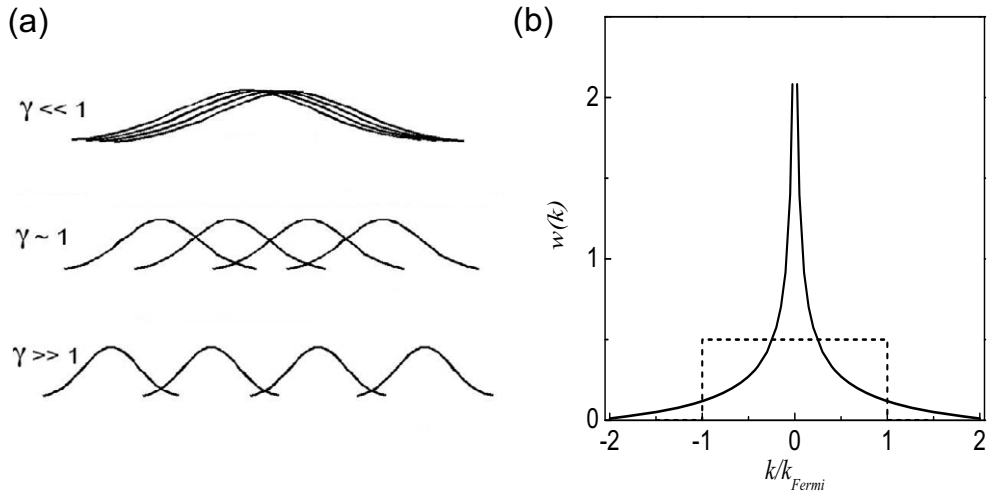

Figure 2.1: (a) Cartoon of atomic density distributions for the Lieb-Liniger gas at $T = 0$ [43]. For increasing values of the interaction parameter γ the interatomic separation increases and the size of the wave-functions decreases. Top: 1D quasi-condensate where atomic waves overlap. Middle: for decreasing density the atomic waves become more localized. Bottom: at very low density the atomic wave-functions exclude each other similar to ideal fermions, for $T = 0$ we have a Tonks-Girardeau gas. (b) Momentum distribution for a Tonks-Girardeau gas of impenetrable bosons at zero temperature (straight line). The corresponding distribution for an ideal Fermi gas is shown for comparison (dashed line). Adapted from Ref. [33].

that the wave-functions of two bosons vanishes when the two atoms are at the same position. Girardeau realized that this is just like the case of ideal fermions, in that case as a result of the exclusion principle. Consequently the ground-state wave-function for interacting bosons ψ^B can be mapped to a system of ideal free spinless fermions ψ^F by multiplying the Fermi wave-function by -1 upon particle exchange. For a ring of length L:

$$\psi^B = |\psi^F| \propto \prod_{j>l} |\sin[\pi L^{-1}(x_j - x_l)]|. \tag{2.42}$$

This wave-function varies smoothly everywhere except for the position where two particles meet, where it vanishes and has a cusp. While the density distribution of these "fermionized" bosons is identical to that of ideal fermions, their momentum distributions $w(k)$ are distinctly different. An analytic rigorous upper bound for $w(k)$ was first given by Lenard [81]. Later the long-range and short-range expansions for $w(k)$ were derived [82, 83]. Following Olshanii [33], we plot $w(k)$ in Fig. 2.1(b). For comparison the momentum distribution for the ideal Fermi case, with $k_F = \pi\,(N-1)\,/L$, is also plotted.

2.5.2 Lieb-Liniger

Lieb and Liniger [35] found the ground-state wave-function for bosons with repulsive delta-function interaction of any strength on a one-dimensional ring (a box of length L with periodic boundary conditions). The Hamiltonian for the Lieb and Liniger system is

$$H = -\frac{\hbar^2}{2m}\sum_{j=1}^{N}\frac{\partial^2}{\partial x_j^2} + g_1\sum_{i>j}\delta(x_i - x_j), \quad g_1 > 0. \tag{2.43}$$

The dimensionless 'Lieb and Liniger' parameter γ is then introduced

$$\gamma = \frac{mg_1}{\hbar^2 n_1}, \tag{2.44}$$

where $n_1 = N/L$. Using the Bethe Ansatz [55] Lieb and Liniger showed that the k's in the Ansatz satisfy

$$(-1)^{N-1}\exp(-ikL) = \exp\left[i\sum_{k'}\theta(k'-k)\right], \tag{2.45}$$

where θ is a phase shift obeying

$$\theta(k) = -2\tan^{-1}(k/\gamma n_1), \quad -\pi < \theta < \pi. \tag{2.46}$$

Lieb [54] also analyzed the excitation spectrum of the Lieb-Liniger gas and found that besides a phonon-like "type I" excitation spectrum, a "type II" branch exist. While the type I excitations match the Bogoliubov phonon spectrum (Sec. 2.4.4) that is valid in the weak coupling limit, the type II excitations do not exist in the Bogoliubov approach. The new branch in the spectrum is associated with "hole-like" excitations: A hole is an omitted k value and is created when a particle with k_i is taken to k_N.

The 1D system shows a peculiar behavior: the system becomes more *strongly* interacting as the density *decreases*. This counter-intuitive effect can be qualitatively understood through the γ parameter. It can be interpreted as the ratio of the interaction energy $\epsilon_{\text{int}} = n_1 g_1$ to the characteristic kinetic energy of the atoms $\epsilon_{\text{kin}} \approx \hbar^2 n_1^2/2m$. Lowering the density, reduces the kinetic energy faster than the interaction energy, thus for low density ($\gamma \gg 1$) we have a strongly interacting gas (Tonks-Girardeau), while in the opposite limit for ($\gamma \ll 1$) we have a weakly interacting gas (1D mean-field).

A nice hybrid theoretical and numerical approach to calculate the excitation spectrum of the Lieb-Liniger gas was taken by Caux and Calabrese [84]. From their results for $0.25 < \gamma < 100$ it becomes clear that for *zero temperature* hole-like excitations are important only for $\gamma \gtrsim 1$. We shall see in the following that already at weak coupling ($\gamma \ll 1$) but for *finite temperature* deviations from the Bogoliubov treatment become important.

2.5.3 Yang-Yang

Yang and Yang [36] extended the Lieb-Liniger treatment to non-zero temperatures. Their method is also known as thermodynamic Bethe Ansatz [37, 38]. Yang and Yang included the effect of thermal excitations by allowing the existence of a whole collection of omitted momentum states (holes), with density $\rho_h(k)$ besides the density of occupied momentum states $\rho(k)$. Yang and Yang were then able to derive analytic expressions for the thermodynamics of this gas. Their main result is formed by the two integral equations

$$\epsilon(k) = -\mu + \frac{\hbar^2 k^2}{2m} - \frac{k_B T g_1}{2\pi} \int_{-\infty}^{\infty} \frac{dq}{(g_1 m/\hbar^2)^2 + (k-q)^2} \ln\left\{1 + \exp\left[-\epsilon(q)/k_B T\right]\right\}, \tag{2.47}$$

where ϵ is defined by

$$\rho_h/\rho = \exp[\epsilon(k)/k_B T], \tag{2.48}$$

and

$$2\pi f(k) = 1 + \frac{2g_1 m}{\hbar^2} \int_{-\infty}^{\infty} \frac{\rho(q)dq}{(g_1 m/\hbar^2)^2 + (k-q)^2}, \tag{2.49}$$

for

$$f(k) = \rho + \rho_h. \tag{2.50}$$

Equation (2.47), where μ is the chemical potential, can be solved for ϵ by iteration. Subsequently ρ can be obtained by iterating Eq. (2.49).

Extra information is obtained [59] by differentiating the free energy per particle FN^{-1} with respect to γ at constant density and temperature

$$g^{(2)} = \frac{2m}{\hbar^2 n_1^2} \left[\frac{\partial(FN^{-1}(\gamma,\tau))}{\partial\gamma}\right]_{n,\tau}, \tag{2.51}$$

where $g^{(2)}$ is the local pair correlation function that expresses the (normalized) probability to find two particles at the same position. In a mean-field condensate, interactions stabilize the density and $g^{(2)} \approx 1$. While ideal bosons experience "bunching" and have $g^{(2)} = 2$, the opposite holds for ideal fermions with $g^{(2)} = 0$ ("anti-bunching"). Fermionized bosons in the TG limit also have $g^{(2)} = 0$.

Figure 2.2(a) shows the numerical solution of the Yang-Yang equations for $1/\gamma \propto n_{YY}$ for different values of the dimensionless temperature parameter

$$t = \frac{2k_B T \hbar^2}{m g_1^2}. \tag{2.52}$$

We plot the values: t=2000 (red), t=1000 (black), t=500 (blue), (numerical data obtained by Kheruntsyan [59, 85]). The exact numerical result (solid lines) is compared with the behavior in the mean-field regime (dashed lines) and with the ideal Bose gas result (dotted lines). The Yang-Yang thermodynamic equations yield a smooth equation of state $n_{YY}(\mu, T)$, including the region around $\mu(x) = 0$. This deviates dramatically from both the ideal-gas description (diverging density as μ approaches zero from below, cf. Eq. (2.22)) and the quasi-condensate description

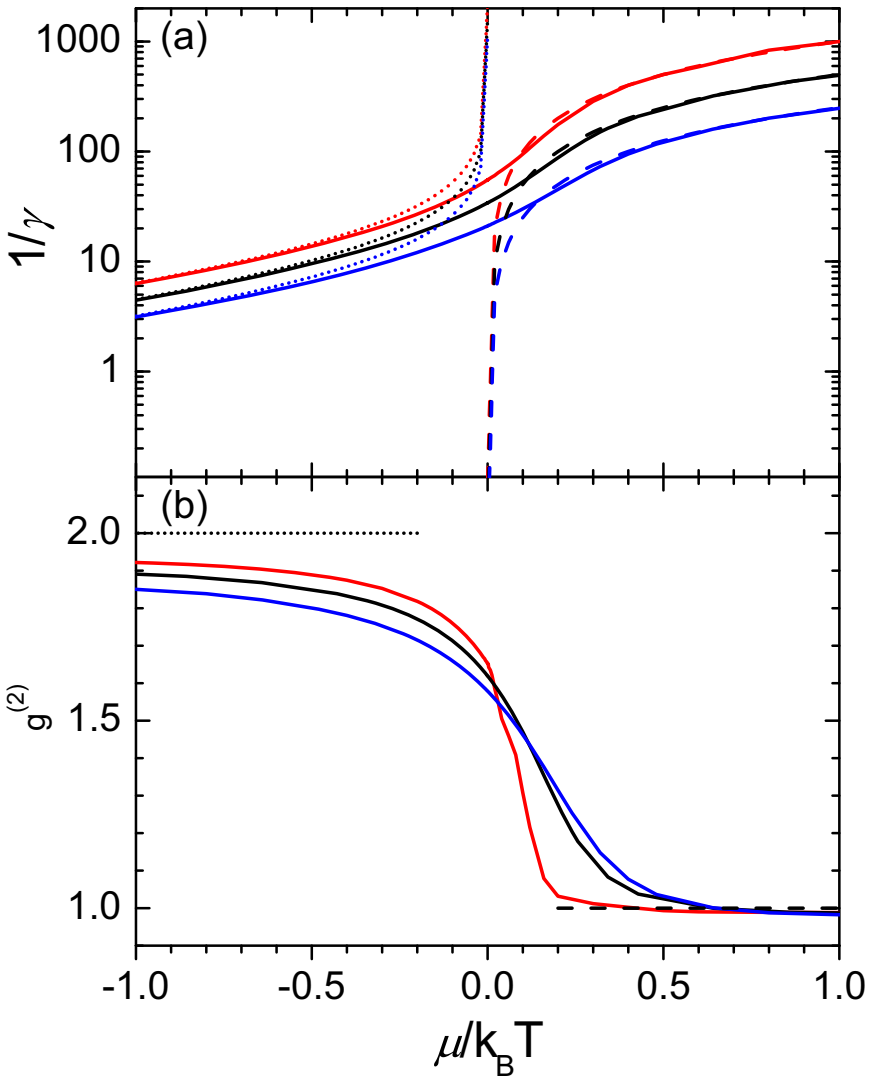

Figure 2.2: (a) Equation of state of the uniform weakly interacting 1D Bose gas for three different values of the temperature parameter $t = 2k_BT\hbar^2/mg_1^2$: t=2000 (red); t=1000 (black); t=500 (blue). The exact numerical result (solid lines) is compared with the behavior in the mean-field regime (dashed lines) and with the ideal Bose gas result (dotted lines). (b) The local correlation $g^{(2)}$ versus μ/k_BT for the same values of t as above. The solid curves are exact numerical results, while the dashed line indicates the mean-field value and the dotted line the behavior of the ideal Bose gas.

($\mu = n_1g_1$; vanishing density as μ approaches zero from above). Hence the exact solutions are crucial for a correct description of the Bose gas in the region around $\mu = 0$ as is described in more detail in Ch. 6.

Fig. 2.2(b) shows the local correlation $g^{(2)}$ versus μ/k_BT for the same values of t as above. The solid curves are exact numerical results, while the dashed line indicates the mean-field value and the dotted line the behavior of the ideal Bose

gas. The calculated value of the local pair correlation function $g^{(2)}$ varies smoothly between ≈ 1 and $\lesssim 2$ in the plotted range of μ. This differs from the ideal-gas value of 2 and the quasi-condensate value of ≈ 1.

2.6 Overview of ultracold Bose gas regimes

2.6.1 Regimes for $T = 0$

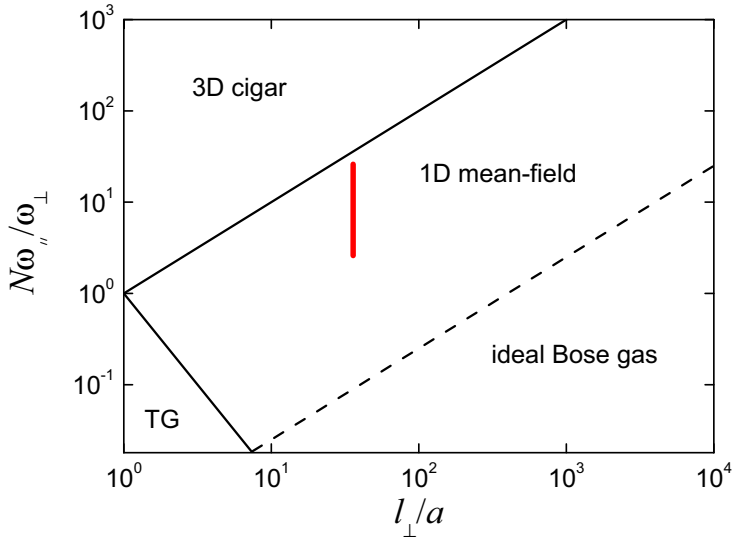

Figure 2.3: Phase diagram for $T = 0$, in the plane $N\omega_{\parallel}/\omega_{\perp}$ versus $l_{\perp}/a$, based on Fig. 1 of Ref. [73]. The dashed line indicates $N\omega_{\parallel}/\omega_{\perp} = (\omega_{\parallel}/\omega_{\perp})^{3/2} l_{\perp}/a$ for $\omega_{\parallel}/\omega_{\perp} = 1/400$. The red line indicates the parameter range covered in our experiment.

The transitions between the various regimes for the $T = 0$ case, that were summarized above, have been studied for a trapped gas by several authors [34, 73]. We follow here the approach by Menotti and Stringari [73]. These authors describe atoms trapped in an elongated harmonic trap with $\omega_{\perp} \gg \omega_{\parallel}$. The longitudinal confinement is weak and for high enough atom number N the atomic interaction energy largely exceeds the axial level splitting ($\mu \gg \hbar\omega_{\parallel}$) and the local density approximation can be used.

A schematic phase diagram is plotted in Fig. 2.3. The line $N\omega_{\parallel}/\omega_{\perp} = l_{\perp}/a$ indicates the cross-over from the 3D cigar from the 1D mean-field regime. Using $\mu = \hbar\omega_{\perp}$ in Eq. (2.36) it follows that this is equivalent to the criterium $n_l = 3/4a$ [74]. The line $N\omega_{\parallel}/\omega_{\perp} = (l_{\perp}/a)^{-2}$ indicates the cross-over from 1D mean-field to the Tonks-Girardeau gas. This demarkation, marked by $\gamma = 1$ in the homogeneous case, is found when the interaction energy equals the kinetic energy: $\pi^2\hbar^2 n_1^2/2m = g_1 n_1$ for the harmonically trapped case, solved in Ref. [73]. The dashed line indicates the cross-over from the parabolic 1D mean-field regime to the ideal gas or gaussian condensate regime where the axial level splitting is large compared to the

atomic interaction energy and the LDA can not be used. We draw the dashed line $N\omega_\parallel/\omega_\perp = (\omega_\parallel/\omega_\perp)^{3/2} l_\perp/a$ for $\omega_\parallel/\omega_\perp = 1/400$, the aspect ratio of the trap used in Chapters 5 and 6. In our experiment we vary the number of atoms in the quasi-condensate between 10^3 and 10^4, while $l_\perp/a = 36$. The covered range is indicated in red in Fig. 2.3. It is clear that the physics of one-dimensional atomic gases plays an important role in our experiments. Secondly, for our aspect ratio we do not reach the TG regime when the atom number is lowered.

2.6.2 Regimes in 1D

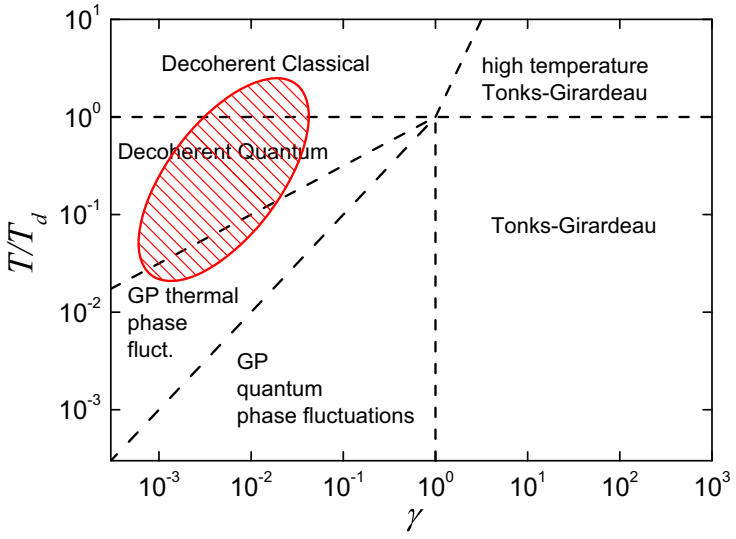

Figure 2.4: Diagram of states for the homogeneous 1D Bose gas in the plane T/T_d versus $\gamma = mg_1/\hbar^2 n_1$. The degeneracy temperature in 1D is given by $T_d = \hbar^2 n_1^2/2mk_B$. The area shaded in red indicates the parameter range covered in our experiment.

The system of delta-function interacting bosons in 1D can be effectively characterized by the combination of the dimensionless coupling parameter γ [Eq. (2.44)] and the reduced temperature $\tau = T/T_d$, with T_d the 1D degeneracy temperature [Eq. (2.23)]. Using the exact values of $g^{(2)}$ [Eq. (2.51)] Kheruntsyan and coworkers [70] have classified various physical regimes for the interacting Bose gas in 1D at finite temperature. The diagram of states is shown in Fig. 2.4. Above the degeneracy temperature two regimes are indicated. For small γ we are in the 'decoherent classical' or non-degenerate ideal Bose gas regime were $g^{(2)} \approx 2$. For large γ, strong interactions result in high temperature fermionization, characterized by $g^{(2)} \to 0$. Below the degeneracy temperature four regimes are distinguished. For $\gamma \gg 1$ we have a degenerate Tonks-Girardeau gas with $g^{(2)} \to 0$. For $\tau \ll \gamma \ll 1$ we have the mean-field regime and the finite temperature correction to the zero-temperature result for the local correlations is small: $g^{(2)} \approx 1$. In this regime quantum fluctuations of the phase dominate over thermal fluctuations. For higher temperatures

$\gamma \ll \tau \ll \sqrt{\gamma}$ we have a mean-field quasi-condensate characterized by thermal fluctuations of the phase, interactions stabilize the density so that $g^{(2)} \gtrsim 1$. If we increase the temperature further $\sqrt{\gamma} \ll \tau \ll 1$ phase coherence is destroyed and we enter the decoherent quantum regime with $g^{(2)} \lesssim 2$. The parameter range covered in the experiments described in this thesis, indicated in red, ranges from the classical regime via the decoherent quantum regime into the mean-field regime.

2.7 Previous models for $T > 0$

2.7.1 Semi-ideal Bose gas

In the situation of a three-dimensional harmonically trapped cloud ($k_B T, \mu \gg \hbar\omega$) just below the condensation temperature $T/T_c \lesssim 1$, the number of non-condensed atoms is large and can not be neglected. In a first approximation [86] we suppose that condensed and non-condensed fractions can be separated spatially because the spatial extent of the BEC is much smaller than that of the thermal cloud so the two parts do not have much spatial overlap. It is further assumed that the BEC is not influenced by the presence of the thermal atoms and maintains its TF profile [Eq. (2.32) and Eq. (2.33)]. The quantum saturated thermal cloud however is repelled by the mean-field interaction energy $2gn_{TF}(\mathbf{r})$ with the much denser condensate in the trap center. The factor 2 accounts for collisions between atoms in *different* quantum states. To find the density distribution of the thermal atoms for this case we use Eq. (2.25) with $D = 3$ that can be written as

$$n_T(\mathbf{r}) = \frac{1}{\Lambda_T^3} g_{3/2}\left[e^{\beta[\mu - V_{\text{eff}}(\mathbf{r})]}\right], \tag{2.53}$$

where we use the effective potential $V_{\text{eff}}(\mathbf{r}) - \mu = V_{\text{ext}}(\mathbf{r}) - \mu_{TF} + 2gn_{TF}(\mathbf{r})$.

2.7.2 Self-consistent Hartree-Fock

When dealing with the system as described in the previous section a more refined approximation can be made by taking into account not only the influence of the condensate on the thermal atoms but also vice versa. This problem can be solved numerically in an iterative process and is referred to as a self-consistent Hartree-Fock (HF) approach [87, 88]. The self-consistent potential for the thermal atoms is

$$V_{\text{eff}}(\mathbf{r}) - \mu = V_{\text{ext}}(\mathbf{r}) + 2gn_0(\mathbf{r}) + 2gn_T(\mathbf{r}) - \mu. \tag{2.54}$$

The condensate profile is affected by the density of the thermal atoms:

$$n_0(\mathbf{r}) = \max\left\{0, \frac{\mu - V_{\text{ext}}(\mathbf{r}) - 2gn_T(\mathbf{r})}{g}\right\}. \tag{2.55}$$

Fixing the total atom number fixes the chemical potential of the thermal fraction $\mu = gn_0(0) + 2gn_T(0)$. This self-consistent HF approach gives accurate results in

the 3D case [89] but has been shown to fail in the description of experimentally obtained profiles when the gas approaches the one-dimensional regime: $k_BT, \mu \simeq 2\hbar\omega_\perp$ [60]. The breakdown of this HF method when approaching the 1D regime and $\mu \approx 0$, can be seen as follows: In 1D, since $g_{1/2}(z) \to \infty$ as $\mu \uparrow 0$ (Sec. 2.3) for any peak density $n(0)$, one can always find a self-consistent HF solution, in the semiclassical approximation for the axial distribution, which has $n_0 = 0$, and $\mu < V_{\rm ext}(0)$. Note also that the local value of the two particle correlation function $g^{(2)}$ differs significantly from both the values 2 and 1 assumed in this approach for the thermal atoms and the condensate atoms respectively (Fig. 2.2).

Luttinger liquid

Another mean-field approach, that will not be discussed further here, is employing the Luttinger liquid (see Haldane [90–93]). It is used mainly for strongly interacting systems and has the same region of validity as Bogoliubov-Popov: $l_\phi \gg l_c$. The Luttinger-liquid approach to one-dimensional Bose gases with delta-function interaction was discussed in detail by Cazalilla [94]. The method has been used successfully to describe the dynamics of phase fluctuations in mean-field condensates [95, 96].

2.8 Evaporative cooling

An important tool in atom cooling that provides the final increase in phase-space density that ultimately leads to Bose-Einstein condensation is evaporative cooling. In this process the high-energy tail of the Maxwell-Boltzmann velocity distribution of the trapped atoms is selectively removed, for example using radio-frequency (RF) induced spin flips. The remaining atoms collide elastically and re-thermalize. The energy per particle decreases and the sample is cooled. Theory describing the evaporative cooling process can be found in [97–100]. We repeat here only the key equations that can be used to calculate the efficiency of the evaporative cooling process. We add specific calculations for the case of the Ioffe-Pritchard trap in the high temperature limit with $\delta = 5/2$ that do not appear in the cited references. A treatment of the IP trap that is valid in the complete range from the high to the low temperature limit can be found in Ref. [100].

If the atomic density of trapped alkali atoms is not too high ($n < 10^{20}$ m^{-3}) three body collisions (that lead to losses via spin exchange) are rare and for typical experiments on alkali atoms the trap lifetime is limited by collisions with background gas. For a trap depth ϵ the truncation parameter is $\eta = \epsilon/k_BT$. Evaporative cooling works most effectively if the truncation parameter η is kept constant. This can be achieved by ramping down the trap barrier during the cooling process, so called forced evaporation. The timescale for evaporative cooling is set by the elastic collision time

$$\frac{1}{\tau_{\rm el}} = \sqrt{2} n_0 v_{\rm th} \sigma, \tag{2.56}$$

where $\sigma = 8\pi a^2$ is the s-wave collisional cross-section and $v_{\rm th} = \sqrt{8k_BT/\pi m}$ the

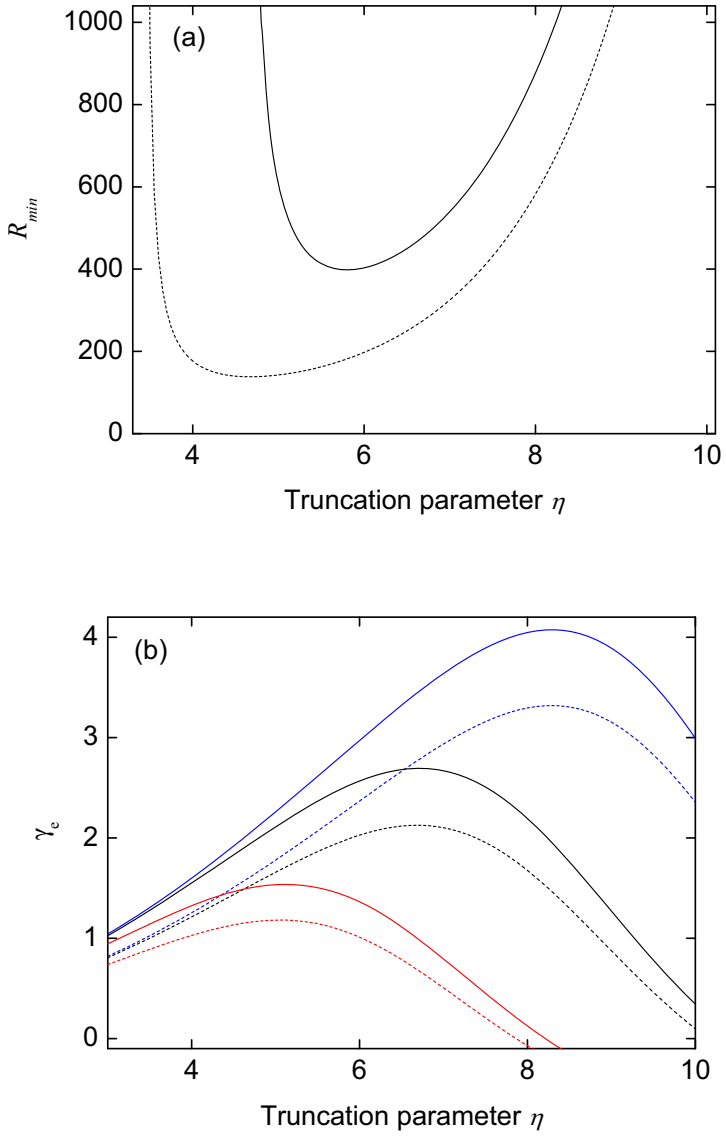

Figure 2.5: (a) Minimum value for the ratio of good to bad collisions plotted as a function of the truncation parameter. Comparison between the 3D parabolic potential ($\delta = 3/2$, solid line) and the 2D linear 1D harmonic potential ($\delta = 5/2$, dashed line). (b) The efficiency parameter of evaporative cooling γ versus the truncation parameter η for $\delta = 3/2$ (solid lines) and $\delta = 5/2$ (dashed lines). In each case, three different lines are given for ratio of good to bad collisions R of 5000 (blue), 1000 (black) and 200 (red).

thermal velocity. For efficient evaporative cooling the ratio R of "good" elastic collisions to "bad" collisions with background gas should exceed a minimal value $R = \tau_{\text{loss}}/\tau_{\text{el}} > R_{\text{min}}$, where τ_{loss} is the trap lifetime. If $R > R_{\text{min}}$ the collision rate increases with decreasing temperature and the regime of run-away evaporation is

entered. Run-away evaporation is most easily reached for steep traps where the density of states decreases rapidly with decreasing temperature as can be seen in the comparison between the 3D harmonic trap [$\delta = 3/2$, Eq. 2.2] and the steeper 1D harmonic 2D linear trap ($\delta = 5/2$) in Fig. 2.5(a). The minimal value for the ratio of good to bad collisions is given by

$$R_{\min}(\delta, \eta) = \frac{\lambda(\delta, \eta)}{\alpha(\delta, \eta)[\delta - 1/2] - 1}, \tag{2.57}$$

where α is the key parameter of the evaporative cooling process, which expresses the temperature decrease per particle lost, and λ is the ratio of the evaporation time to the elastic collision rate. The parameters α and λ can be calculated using the following expressions.

Used below are the incomplete gamma functions P and R, defined as (see appendix in Ref. [98])

$$P(a, \eta) = \frac{1}{\Gamma(a)} \int_0^\eta t^{a-1} e^{-t} dt, \tag{2.58}$$

$$R(a, \eta) = \frac{P(a+1, \eta)}{P(a, \eta)}, \tag{2.59}$$

where $\Gamma(a)$ is the Euler gamma function. The average energy of the escaping atoms is $(\eta + \kappa)k_B T$, where the parameter κ for the case of a power-law trap is

$$\kappa = 1 - \frac{P(7/2 + \delta, \eta)}{\eta P(3/2 + \delta, \eta) - (5/2 + \delta) P(5/2 + \delta, \eta)}. \tag{2.60}$$

This leads to an expression for α for forced evaporative cooling at constant η (see p. 194 of Ref. [99])

$$\alpha(\delta, \eta) = \frac{\eta + \kappa(\delta, \eta) - [3/2 + \tilde{\gamma}(\delta, \eta)]}{3/2 + \tilde{\gamma}(\delta, \eta) + \kappa(\delta, \eta)[\delta - \tilde{\gamma}(\delta, \eta)]}, \tag{2.61}$$

where the scaling parameter $\tilde{\gamma}$ [see Ref. [98], Eq. (99)] for a power-law trap is

$$\tilde{\gamma} = -\frac{3}{2} + \left(\frac{3}{2} + \delta\right) R(3/2 + \delta, \eta). \tag{2.62}$$

Finally, the parameter λ, expressing the ratio of the evaporation time to the elastic collision rate is given by

$$\lambda(\delta, \eta) = \left(1 - \left[\frac{3}{2} + \delta\right] [1 - R(3/2 + \delta, \eta)]\, \alpha(\delta, \eta)\right) \frac{\sqrt{2} \exp(\eta)}{\eta - (5/2 + \delta) R(3/2 + \delta, \eta)}. \tag{2.63}$$

Once the condition $R > R_{\min}$ is fulfilled it is useful to calculate the overall figure of merit for the effectiveness of the evaporation process given by the parameter $\gamma_{\mathrm{e,tot}}$, that expresses the relative increase in phase space density with decreasing atom number

$$\gamma_{\mathrm{e,tot}} = \frac{\ln(\Phi_{\mathrm{final}}/\Phi_{\mathrm{initial}})}{\ln(N_{\mathrm{final}}/N_{\mathrm{initial}})}. \tag{2.64}$$

This global parameter is maximal when $\gamma_e = -d(\ln \Phi)/d(\ln N)$ is optimized at all times. From Eq. (10) of Ref. [99] we find

$$\gamma_e(\delta, \eta, R) = \frac{\alpha(\delta, \eta)[\delta + 3/2]}{1 + \lambda(\delta, \eta)/R} - 1. \tag{2.65}$$

The calculated values of γ_e for the cases $\delta = 3/2$ and $\delta = 5/2$ are plotted in Fig. 2.5(b). In the case $\delta = 5/2$ for $R = 1000$ the overall maximal efficiency $\gamma_e = 2$, provided $\eta \approx 7$. This means that a typical gain of 6 orders of magnitude in phase space density costs 3 orders of magnitude in atom number.